Richard W. Hammond[1]
Joel S. Bader[1]
Steven A. Henck[1]
Michael W. Deem[1*]
Gregory A. McDermott[1]
James M. Bustillo[2]
Jonathan M. Rothberg[1]

[1]CuraGen, New Haven, CT, USA
[2]Department of Electrical Engineering and Computer Science, University of California, Berkeley, CA, USA

Differential transport of DNA by a rectified Brownian motion device

An interdigitated electrode array (IDEA) device has been designed and used to transport DNA based on a Brownian ratchet mechanism. This migration is produced by the periodic formation of an asymmetric sawtooth electric field in the device. Oligonucleotides of 25, 50, and 100 bases in length were tested using two different array geometries. DNA transport as a function of DNA size, electric field frequency, and array geometry is shown to be in qualitative agreement with theory. Such a device could provide for DNA separations over a broad size range, and can be readily scaled as a component in a microfabricated DNA analysis system.

Keywords: DNA / Microdevices / Microfabrication / Brownian ratchet EL 3737

1 Introduction

The Human Genome Project and similar efforts are providing a wealth of genetic information that is spurring a rapid growth in the number of nucleic acids-based diagnostic tests which can be performed on a routine basis in hospitals or forensic laboratories [1, 2]. Much work in recent years has shown the feasibility of using microfabrication techniques to produce integrated "lab-on-a-chip" devices for DNA separations, which offer the advantages of higher throughput at lower costs [3–10]. Such microfabricated devices have been demonstrated for capillary electrophoresis, as well as performing chemical reactions, including solid-phase chemistry, polymerase chain reaction, immunoassays, and cell manipulations [3]. Another key for improving such diagnostics using miniaturized biochemical analysis systems will be their simplicity of operation. DNA separations in microdevices to date have been accomplished by means of standard electrophoretic methods. This requires the use of a polymer solution as a sieving matrix [11]. The use of such solutions can become more complicated as channel dimensions decrease [4]. Experiments showing DNA separations in free solution have been performed but required precisely controlled modification of the DNA molecules [12]. It has also been proposed that devices for specific DNA separations could be created using a microfabricated array of posts for DNA sieving [13]. Ideally, a microdevice would separate molecules over a wide size range, with the specificity controlled simply by adjustable instrumental parameters.

Directed motion by means of "Brownian ratchets" has been discussed extensively [14–21], and used to describe the mechanism of molecular motors [22–25]. Brownian motion is rectified when a time-dependent energy source is applied in an anisotropic environment. Recently, the sorting of macromolecules by a continuous flow through an array of obstacles asymmetric in both *x* and *y* dimensions has been suggested [26–29]. Experimentation using Brownian ratchets has involved the migration of relatively large objects using dielectrophoresis [30, 31] or optical tweezers [32] to generate the periodic, asymmetric potential energy field. Such energy fields have been too weak for directed motion of smaller, less polarizable DNA fragments.

Elsewhere, we have described the development and use of a Brownian ratchet microdevice for the directed motion of DNA molecules [33]. Figure 1 shows a schematic of our operating device. The device uses charge-charge interactions to create the anisotropic potential energy field, which allows the trapping of smaller particles such as DNA fragments. The device consists of two asymmetric arrays of electrodes. The array geometry is defined by the periodicity between anodes, *l*, and the minimum distance between anode and cathode, *r*. The design is such that $l >> r$. The anisotropic potential energy field is created by applying voltage to the arrays for a period of time t_{on} sufficient to localize the negatively charged DNA fragments to a potential energy minimum. The voltage is subsequently turned off for a period of time t_{off}, permitting Brownian diffusion of the DNA fragments about the formerly defined potential energy minimum. Modeled in one dimension the probability distribution of DNA about this point is Gaussian,

$$P(x;t_{off}) = \frac{\exp(-x^2/4Dt_{off})}{\sqrt{4\pi Dt_{off}}} \quad (1)$$

Correspondence: Dr. Richard W. Hammond, CuraGen, 555 Long Wharf Drive, New Haven, CT 06511, USA
E-mail: rhammond@curagen.com
Fax: +203-401-3351

Abbreviation: IDEA, interdigitated electrode array

* Present address: Department of Chemical Engineering, University of California, Los Angeles, CA 90095, USA

 0173-0835/00/0101-0074 $17.50+.50/0

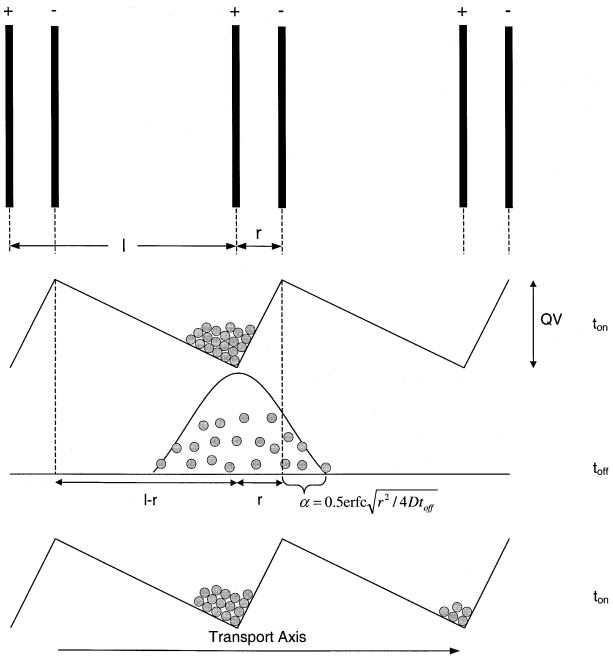

Figure 1. Example of Brownian ratchet operation. A periodic potential is applied to the electrode array. Charged particles with diffusion coefficient *D* focus to the potential well minima during period t_{on}. During period t_{off} a fraction of the particles α diffuse beyond a distance *r*, which can be quantified from the complementary error function of the particle distribution. Subsequent cycling of the potential generates a net transport of the particles.

where *D* is the diffusion coefficient for the DNA fragment. The period of time t_{off} is optimized to permit a fraction α of the DNA to migrate a distance such that $l\text{-}r > x > r$. This fraction α can be expressed by integrating the probability distribution function from *r* to infinity:

$$\alpha = \frac{1}{2}\,\mathrm{erfc}\left(\sqrt{r^2/4Dt_{off}}\right) \qquad (2)$$

where erfc *x* is the error function complement. Voltage cycling between t_{on} and t_{off} produces a net transport of DNA fragments of αl after each cycle. A migrating distribution for each fragment size is therefore produced after *n* cycles, with center position *x (n)*,

$$x(n) = nl\alpha \qquad (3)$$

and square width $\sigma^2(n)$,

$$\sigma^2(n) = nl^2\alpha(1-\alpha) \qquad (4)$$

In this report, we perform a more detailed characterization of the device by investigating a more complete set of parameters. In particular, we transport oligonucleotides 25–100 bases in length using two different device geometries. The transport rates, as a function of oligonucleotide size, further support our previous conclusions. These results also show qualitative agreement between theoretical prediction and actual performance of the physical device. We also use the dependence of the transport rate on oligonucleotide size to predict the resolution that can be obtained for DNA separations. Also, we use the data from different device feature sizes to test the theoretical prediction that the cycle time can be reduced with the square of the feature size. This test is crucial because reducing feature size is the most direct means to improve performance and resolution.

2 Materials and methods

2.1 Device fabrication and preparation

The design of the interdigitated electrode array (IDEA) device is shown in Fig. 2. The device consists of two asymmetrically spaced electrode arrays extending from platinum bondpads on opposite sides of the device. The asymmetry is defined by the periodicity, *l*, and the spacing between nearest electrodes, *r*, which also defines the electrode width. Devices with two different geometries were fabricated, one with *r* and *l* equal to 5 and 50 μm, respectively (5/50 device), the other with *r* and *l* equal to 2 μm and 20 μm, respectively (2/20 device).

The IDEA device was produced at the UC Berkeley Microfabrication Laboratory using conventional microelectronic fabrication techniques involving photolithographic patterning and etching of deposited or grown thin-films [34–36]. The methods employed are characteristic of those commonly used in the integrated circuit industry and lend themselves to high-density, low-cost batch fabrication. IDEA devices were fabricated on 100 mm diameter silicon wafers, on which over 100 distinct devices can be produced simultaneously. Fabrication begins with a dielectric layer, formed by the thermal oxidation of the silicon surface. An adhesion layer to bond the metal to the substrate is then applied. This is followed by a 2000 Å layer of platinum, which was used for the device metallurgy. This was deposited in an radio frequency (RF)-magnetron sputtering system with an argon gas ambient. Photolithography is then used to define the platinum electrodes and bondpads. The photolithographic mask is shown in Fig. 2a. Because of its highly inert nature, platinum is difficult to remove using conventional reactive ion plasma techniques; argon ion milling was therefore used to remove the exposed platinum. To limit DNA adsorption, the devices were treated with an organosilane before use. Devices were soaked in isopropanol followed by isooctane. The devices were then placed in a silanization

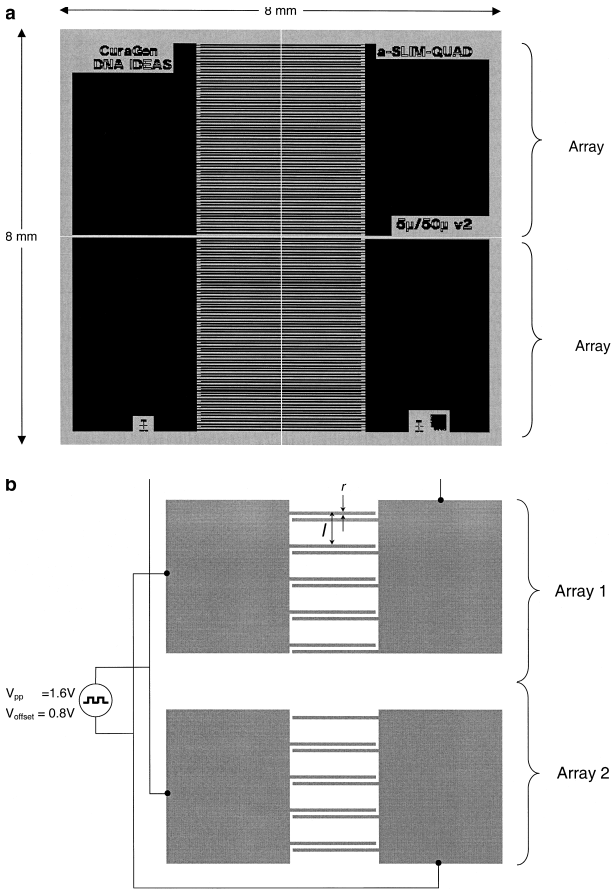

Figure 2. (a) Photolithographic mask for the 5/50 IDEA device. (b) Device schematic, showing connection of the power supply and array dimensions *l* and *r*. For the 5/50 device*l* = 50 μm and *r* = 5 μm. For the 2/20 device *l* = 20 μm and *r* = 2 μm. The voltage waveform is at 25% duty cycle. The initial voltage polarity transports DNA to the center of the device, concentrating the DNA to the lone anode in array 2. Reversal of the voltage polarity produces in both electrode arrays a band of DNA migrating from the device center outwards.

bath consisting of 80 mL hexadecane, 20 mL chloroform, and 80 mL of methacryloxypropyltrichlorosilane (Gelest, Tullytown, PA). The devices were soaked in this silanization bath for 20 min. The devices were then rinsed consecutively in iso-octane, isopropanol, and water, followed by drying under nitrogen.

2.2 Reagents and samples

Oligonucleotides of length 25 bases (5'-GCA TCA CAG TCA GTA GCA TCA GGT C-3'), 50 bases (5'-TCG TCC TGT CAG ACG AGA CTG CTG ACG ACA TCT ATC ATC GGT ATC TGC CG-3'), and 100 bases (5'-TCG TCC TGT CAG ACG AGA CTG CTG ACG ACA TCT ATC ATC GGT ATC TGC CGT CGT CCT GTC AGA CGA GAC TGC TGA CGA CAT CTA TCA TCG GTA TCT GCC G-3'), labeled at the 5'-end with carboxy-X Rhodamine, were custom synthesized (Amitof, Allston, MA). The base sequences were chosen to prevent hairpinning and self-hybridization. MALDI-MS analysis of the oligonucleotides showed no evidence of incomplete synthesis products. These oligonucleotides were used at a concentration of 0.1 pmol/μL.

2.3 Instrumentation

An epi-illumination microscope (Zeiss Axioskop, Jena, Germany), using a 10X Fluar objective was used for imaging. The device was illuminated by a 50 W mercury lamp, using a 546 nm bandpass excitation filter and 590 nm longpass emission filter. Visualization of the DNA dynamics was by means of an intensified video camera (SIT camera Model VE-1000; Dage-MTI, Michigan City, IN) attached to the microscope, with results recorded by videotape. The standard video frame rate of 30 fps allowed for sufficient sampling of the electric field frequencies used in the experiments. A function generator (Model DS345; Stanford Research Systems, Sunnyvale, CA) created the electric field waveform, which was then applied directly to the device by means of probe contacts to the device bondpads. The electric field waveform used in the experiments was a square wave with voltage amplitude V_{pp} = 1.6 V, 25% duty cycle ($t_{off} = 3t_{on}$), and 0.8 V offset. Frequencies for the electric field ranged from 0.7 to 8 Hz, with $\nu=(t_{off}+t_{on})^{-1}$.

2.4 Procedure

For the experiment 0.15 μL of DNA solution was applied to the device, over which a 2 × 5 mm coverslip was placed, creating a maximum solution depth of approximately 15 μm. The coverslip edge was then sealed to the device with grease to prevent bulk flow. Voltage was applied to the two electrode arrays by probe contact with the bondpads in such a manner that DNA migration for each array was in opposing directions. The initial polarity was set to drive DNA motion on each array towards the center of the device, where it concentrated on the center anode. After 2 min the polarity of the electric field for both arrays is inverted, creating two concentrated bands of DNA which migrate from the device center to the edges. A total of 88 runs were analyzed for this report.

2.5 Analysis

Digitization of the videotape was by means of a PCI frame grabber (Model DT3153; Data Translation, Marlboro, MA) in a Pentium PC, operated *via* image processing software (HLImage; Western Vision Software, Layton, UT). A

region of interest 8 pixels wide and covering the length of an array was captured at a frequency equal to that of the electric field used, in phase with t_{on}. A total of 100 frames were captured for each run. To remove background the brightest 15% of the pixels were used to determine the location of the DNA bands. DNA band migration, *x(n)*, was measured as the average position as weighted by intensity. Values of α were calculated as the slope of *x(n)*, using frames 10 through 39.

3 Results and discussion

3.1 Typical run

In Fig. 3, we show results from a typical run. Here the labeled 50-mer is transported on a 2/20 device. The electric field frequency is 0.7 Hz. The top panel shows images of the device region of interest at 10-frame intervals. The bright bands show DNA that has been attracted to the array anodes, which are the potential well minima. After each cycle of the electric field, a fraction α of DNA progresses to the next array anode. This produces an advancing DNA band spread out over several anodes. Visual inspection of the images shows the band migrating approximately two anode positions, or *2l*, every ten electric field cycles. This yields a value for α of 0.2. The migration and spread of the 50-mer band is plotted below the images. When measured as the slope of *x(n)*, the value of α is 0.19. Also plotted is the band width, expressed as $\sigma^2(n)$. From Eq. (3), the slope of $\sigma^2(n)$ is equal to $\alpha(1\text{-}\alpha)$ = 0.15, or approximately equal to the slope for *x(n)*. After 25 cycles $\sigma^2(n)$ becomes linear with a slope equal to 0.15, in agreement with theory. The goodness of fit, however, is poor (R^2=0.6), due to the high fluorescence background in our device.

3.2 Dependence of α on electric field frequency and diffusion distance

Figure 4 shows experimental results of α for the labeled 50-mer as a function of frequency, using both the 5/50 and 2/20 device geometry. It can be seen that α increases as near electrode spacing *r* decreases, as predicted by theory. The steady-state flux of particles through the device can be expressed as

$$\text{flux} = \alpha\nu \tag{5}$$

From visual observation, frequencies yielding maximum flux for the two different devices were 0.7 Hz and 2 Hz, respectively*. To determine if the data qualitatively follows the theoretical functional form, the function for the flux was optimized to have a maximum at the stated frequencies. One manner in which the experimental data could deviate from theoretical is in the values for *r*. The simplified one-dimensional model does not account for the electrode width. The actual distance necessary for the DNA to diffuse across to the next potential well may be better approximated by the center-to-center distance between near electrodes,

$$r = 2r_{phys} \tag{6}$$

or from the near-edge-to-far-edge distance between near electrodes.

$$r = 3r_{phsy} \tag{7}$$

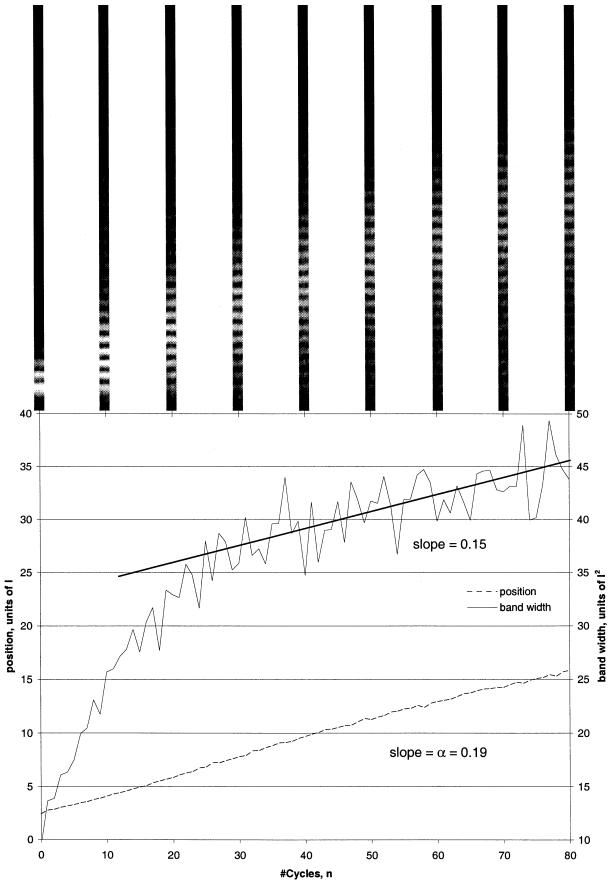

Figure 3. Top: images of 50-mer migration on 2/20 device, in 10 cycle intervals. Voltage waveform as in Fig. 2, with ν=0.7 Hz. Bottom: band migration *x* and band width as σ^2, plotted relative to the number of cycles, *n*. The value for α is calculated as dx/dn. The function σ^2 becomes linear after *n*=25, and $d\sigma^2/dn \cong \alpha(\alpha\text{-}1)$, as predicted by theory.

* Experiments for the 50-mer using the 5/50 device were performed at several other frequencies. However, the device preparation was different. Therefore, these data are not included in Fig. 4.

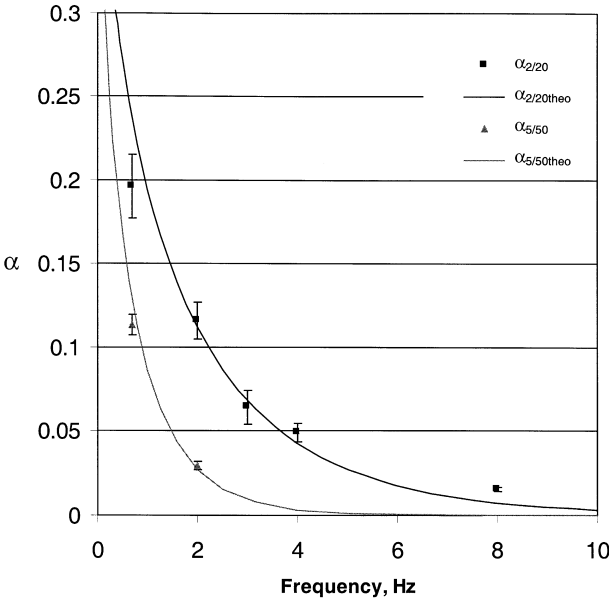

Figure 4. Dependence of α on electric field frequency, measured for both 2/20 and 5/50 devices. Theoretical curves include correction factors $s_{2/20}$ and $s_{5/50}$, based on the frequency of maximum DNA flux. The error bars indicate 1σ.

The function for the flux was therefore optimized by means of including a correction factor *s* to *r*:

$$r = sr_{phys} \tag{8}$$

The diffusion coefficient *D* was determined assuming that the oligonucleotide behaves as a self-avoiding Gaussian chain, that is:

$$D \sim L^{-0.6} \tag{9}$$

where *L* is the chain length in bases. Previous work has shown that values for the diffusion coefficient decrease in micron-sized environments [37]. Xu and Yeung, by means of single molecule detection, calculated a diffusion coefficient of 2.5×10^{-7} cm^2/s for dye-labeled 30-mer. This is a factor of 2.6 less than the value based on the Stokes-Einstein equation. Using the scaling from Eq. (8) relative to this value, the diffusion coefficient for a 50-mer would be 1.8×10^{-7} cm^2/s. For the 25% duty cycle square wave, t_{off} can be expressed as

$$t_{off} = 0.75/\nu \tag{10}$$

Substitution into Eq. (1) then yields

$$\alpha = \frac{1}{2}\,\mathrm{erfc}\left(\sqrt{s^2 r^2 \nu / 3D}\right) \tag{11}$$

A value for *s* that optimized DNA flux for the above frequencies was determined. The correction factor *s* was different for each device, however both are close to the range limit we expected, being $s_{2/20} = 3.6$ and $s_{5/50} = 2.2$. The functions $\alpha_{2/20}(\nu)$ and $\alpha_{5/50}(\nu)$ using these correction factors are overlaid on the experimental data. The data show good agreement with these functions.

Runs were also performed on both the 2/20 and 5/50 devices using labeled 25-mer and 100-mer oligonucleotides. These data points can be added to the 50-mer data if we scale the data sets to account for the oligonucleotide size. Using the scaling for the diffusion coefficient expressed in Eq. (8), values for the other oligonucleotides were determined as follows:

$$D_{oligo} = D_{50mer}\left(\frac{50}{L}\right)^{0.6} \tag{12}$$

Data for all three oligonucleotides were combined, and α was plotted as a function of ν/D_{oligo}. This is shown in Fig. 5, overlaid with the theoretical curves. The data generally follow the functional form. However, values of α for the 25-mer and 100-mer tend to show greater deviation. This could be an expression of how the DNA size range used less accurately reflects a self-avoiding random walk model. No account is made for the intrinsic chain stiffness. This is often expressed in terms of statistical segment length, or Kuhn length, b_K. A Gaussian chain accurately models a DNA molecule when $L >> b_K$ [38]. For ss-DNA, the Kuhn length is approximately 4 nm [39]. Values of L/b_K for the oligonucleotides used therefore range from 2–8. The diffusion coefficient for such semiflexible, shorter chains is more dependent on the chain length *L*

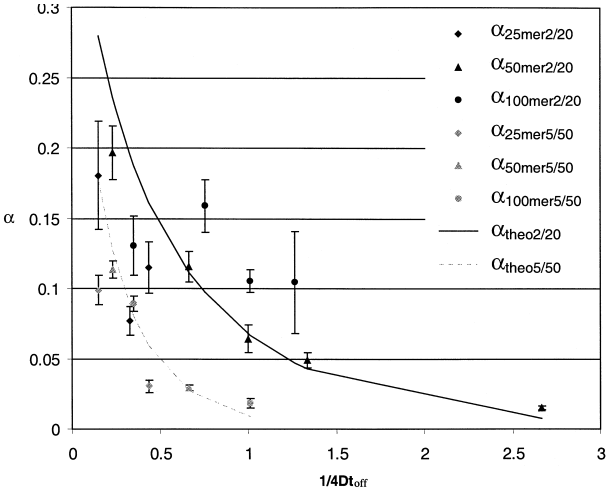

Figure 5. Dependence of α on the diffusion distance *r*, independent of oligonucleotide size. Theoretical curves include the appropriate correction factor, $s_{2/20}$ or $s_{5/50}$. The error bars indicate 1σ.

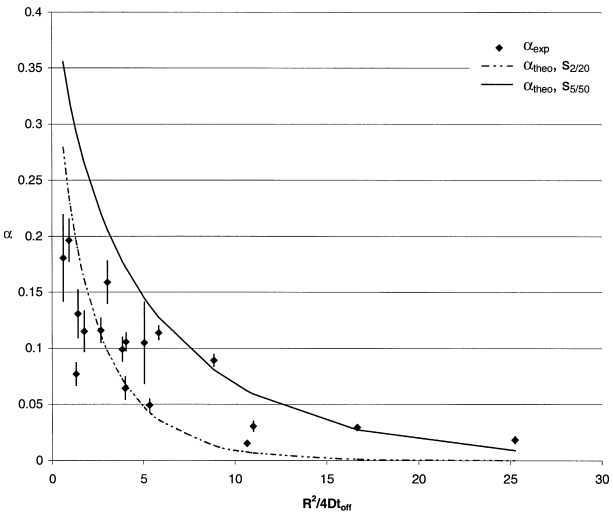

Figure 6. Values of α fit to the single parameter $r^2/4Dt_{off}$. The theoretical curves include the appropriate correction factor, $s_{2/20}$ or $s_{5/50}$. The error bars indicate 1σ.

than expressed by the self-avoding random walk model [40]. An optimization based on data for the 50-mer could therefore be less accurate for the other oligonucleotides. Data from all oligonucleotides are shown together in Fig. 6. Here α is plotted as a function of $r^2/4Dt_{off}$. All data should follow one functional form. This curve is overlaid on the data, one using $s_{2/20}$, the other using $s_{5/50}$. This is reasonable since two-thirds of the data points were obtained using the 2/20 device.

3.3 Sample interaction with electrode array

Another factor contributing to deviation from theory comes from the interaction of the samples with the electrode array. In our experiments the DNA solution is in direct contact with the platinum electrodes. Specific adsorption of analytes and other solution constituents onto solid electrodes is a general phenomena [41, 42]. The resultant electrode fouling diminishes the effective electric field in the device. DNA, particularly single-stranded, has been shown to be adsorbed onto gold and carbon electrodes [43–45]. The degree of adsorption increases with shorter DNA size, as these shorter chains can more readily follow the contours of the electrode surface [43]. The guanine and adenine bases are also susceptible to oxidation over the potential range used in our experiments [46–49]. Adsorption of the DNA with resultant weakening of the electric field was observed during the operation of the device. With extended operation, the background fluorescence on the electrodes would increase, producing DNA bands of decreasing signal/noise. After 8 min of operation, the combination of high background and diminished electric field prevented further observation of DNA migration.

3.4 Dependence of α on oligonucleotide size

Figure 7 shows the dependence of α on oligonucleotide size for both the 2/20 and 5/50 device. While there is a clear decrease in α with size between the 50-mer and 100-mer, values of α for the 25-mer were lower than predicted, and in fact often lower than for the 50-mer. This again could be attributable to a greater degree of adsorption for the 25-mer relative to the 50-mer and 100-mer.

4 Concluding remarks

These preliminary results show the utility of using a Brownian ratchet mechanism for the transport of DNA. This Brownian ratchet device provides some attractive advantages over electrophoresis for DNA separations. It does not require the use of polymer solutions to effect separation. Since the separation window is dependent on the electric field frequency, the same device could be used to separate a wide range of sizes, providing great flexibility. The device is capable of being readily included into present techniques used to develop integrated microdevices. The electrode dimensions for this device could be decreased and greatly improve resolution. With the present technology used in the microelectronics industry, device features of 0.25 μm are routinely achieved [50]. The experiments, reproduced for multiple oligonucleotide sizes under varying operational parameters, are in qualitative agreement with theory. Our use of correction factors, however, shows that a more refined model for the transport is necessary. A two-dimensional model that takes into account the finite electrode width will allow for a more accurate determination of the potential well parame-

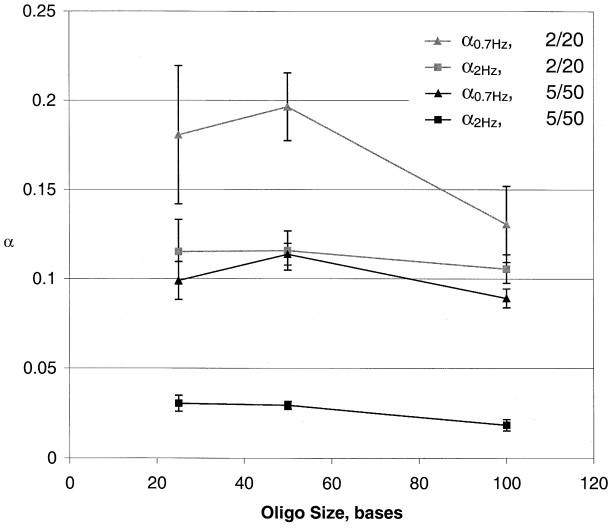

Figure 7. Dependence of α on oligonucleotide size. The theoretical curves include the appropriate correction factor, $s_{2/20}$ or $s_{5/50}$. The error bars indicate 1σ.

ters. What will also be necessary is a treatment of the electrode arrays to prevent adsorption of the DNA and other contributions to electrode fouling. With these improvements this device could provide a feasible alternative to electrophoresis for nucleic acid separations.

We wish to acknowledge the support of SBIR grant 1 R43 HG01535-01 from the National Human Genome Research Institute and Advanced Technology Program award 1966-01-0141 from the National Institute of Standards and Technology.

Received June 23, 1999

5 References

[1] Fleischmann, R. D., Adams, M. D., White, O., Clayton, R. A., Kirkness, E. F., *Science* 1995, *269*, 496–512.

[2] Wagener, C., *J. Mol. Med.* 1997, *75*, 728–744.

[3] Khaledi, M. G., (Ed.), *High Performance Capillary Electrophoresis*, John Wiley & Sons, New York 1998, pp. 613–633.

[4] Mastrangelo, C. H., Burns, M. A., Burke, D. T., *Proc. IEEE* 1998, *86*, 1769–1786.

[5] Burns, M. A., Johnson, B. N., Brahmasandra, S. N., Handique, K., Webster, J. R., Krishnan, M., Sammarco, T. S., Man, P. M., Jones, D., Heldsinger, D., Mastrangelo, C. H., Burke, D. T., *Science* 1998, *282*, 484–487.

[6] Colyer, C. L., Tang, T., Chiem, N., Harrison, D. J., *Electrophoresis* 1997, *18*, 1733–1741.

[7] Manz, A., Harrison, D. J., Verpoorte, E., Widmer, H. M., *Adv. Chromatogr.* 1993, *33*, 1–66.

[8] Woolley, A. T., Mathies, R. A., *Proc. Natl. Acad. Sci. USA* 1994, *91*, 11348–11352.

[9] Jacobson, S. C., Hergenroder, R., Koutny, L. B. Ramsey, J. M., *Anal. Chem.* 1994, *66*, 2369–2373.

[10] Wilding, P., Shoffner, M. A., Kricka, L., *J. Clin. Chem.* 1994, *40*, 1815–1818.

[11] Cohen, A. S., Najarian, D. R., Paulus, A., Guttman, A., Smith, J. A., Karger, B. L., *Proc. Natl. Acad. Sci. USA* 1988, *85*, 9660–9663.

[12] Heller, C., Slater, G. W., Mayer, P., Dovichi, N., Pinto, D., Viovy, J. L., Frouin, G., *J. Chromatogr.* 1998, *806*, 113–121.

[13] Duke, T., Monnelly, G., Austin, R. H., Cox, E. C., *Electrophoresis* 1997, *18*, 17–22.

[14] Astumian, R. D., *Science* 1997, *276*, 917–922.

[15] Astumian, R. D., Bier, M., *Phys. Rev. Lett.* 1993, *72*, 1766–1769.

[16] Doering, C. R., Horsthemke, W., Riordan, J., *Phys. Rev. Lett.* 1994, *72*, 2984–2987.

[17] Magnasco, M. O., *Phys. Rev. Lett.* 1993, *71*, 1477–1480.

[18] Prost, J., Chauwin, J. F., Peliti, L., Ajdari, A., *Phys. Rev. Lett.* 1994, *72*, 2652–2655.

[19] Tarlie, M. B., Astumian, R. D., *Proc. Natl. Acad. Sci. USA* 1998, *95*, 2039–2043.

[20] Julicher, F., Ajdari, A., Prost, J., *J. Rev. Mod. Phys.* 1997, *69*, 1269–1304.

[21] Astumian, R. D., Bier, M., *Biophys. J.* 1996, *70*, 637–653.

[22] Astumian, R. D., *J. Phys. Chem.* 1996, *100*, 19075–19081.

[23] Howard, J., Hudspeth, A. J., Vale, R. D., *Nature* 1989, *342*, 154–156.

[24] Kuo, S. C., Sheetz, M. P., *Science* 1993, *260*, 232–234.

[25] Svoboda, K., Schmidt, C. H., Schnapp, B. J., Block, S. M., *Nature* 1993, *365*, 721–723.

[26] Duke, T. A., Austin, R. H., *Phys. Rev. Lett.* 1998, *80*, 1552–1555.

[27] Ertas, D., *Phys. Rev. Lett.* 1998, *80*, 1548–1551.

[28] Slater, G. W., Guo, H. L., Nixon, G. I., *Phys. Rev. Lett.* 1997, *78*, 1170–1173.

[29] Derenyi, I., Astumian, R. D., *Phys. Rev. Lett.* 1998, *58*, 7781–7784.

[30] Gorre, L., Ioannidis, E., Silberzan, P., *Europhys. Lett.* 1996, *33*, 267–272.

[31] Rousselet, J., Salome, L., Ajdari, A., Prost, J., *Nature* 1994, *370*, 446–448.

[32] Faucheux, L. P., Bourdieu, L. S., Kaplan, P. D., Libchaber, A. J., *Phys. Rev. Lett.* 1995, *74*, 1504–1507.

[33] Bader, J. S., Hammond, R. W., Henck, S. A., Deem, M. W., McDermott, G. A., Simpson, J. W., Mulhern, G. T., Rothberg, J. M., *Proc. Natl. Acad. Sci. USA* 1999, in press.

[34] Chang, C. Y., Sze, S. M., *ULSI Technology*, McGraw-Hill, New York 1996.

[35] Sze, S. M., *VLSI Technology*, McGraw-Hill, New York 1988.

[36] Wolf, S., Tauber, R. N., *Silicon Processing for the VLSI Era*, Lattice Press, Sunset Beach, CA 1990.

[37] Xu, X.-H., Yeung, E. S., *Science* 1997, *275*, 1106–1109.

[38] Doi, M., Edwards, S., *The Theory of Polymer Dynamics*, Clarendon, Oxford 1986, p. 100.

[39] Grosberg, A. Y., Khokhlov, A. R., *Statistical Physics of Macromolecules*, AIP Press, New York, p. 301.

[40] Yamakawa, H., Fujii, M., *J. Chem. Phys.* 1976, *64*, 5222.

[41] Bard, A. J., Faulkner, L. R., *Electrochemical Methods*, John Wiley & Sons, New York 1980, pp. 488–546.

[42] Adams, R. N., *Electrochemistry at Solid Electrodes*, Marcel Dekker, New York 1969, pp. 187–208.

[43] Brown, G. M., Allison, D. P., Warmack, R. J., Jacobson, K. B., Larimer, F. W., Woychik, R. P., Carrier, W. L., *Ultramicroscopy* 1991, *38*, 253–264.

[44] Brett, C. M. A., Brett, A. M. O., Serrano, S. H. P., *J. Electroanal. Chem.* 1994, *366*, 225–231.

[45] Lindsay, S. M., Tao, N. J., DeRose, J. A., Oden, P. I., Lyubchenko, Y. L., Harrington, R. E., Shlyakhtenko, L., *Biophys. J.* 1992, *61*, 1570–1583.

[46] Wang, J. W., Cai, X., Jonsson, C., Balakrishnan, M., *Electroanalysis* 1996, *8*, 20–24.

[47] Brabec, V., *Biophys. Chem.* 1979, *9*, 289–297.

[48] Brabec, V., *J. Electroanal. Chem.* 1980, *116*, 69–82.

[49] Palecek, E., *Electroanalysis* 1996, *8*, 7–14.

[50] Sun, J. Y. C., Chiang, S.-Y., Liu, M., *International Electron Devices Meeting 1998 Technical Digest*, San Francisco, CA, December 1998, pp. 321–324.